Molecular Microbiology (2009) 71(3), 702–716 ■
doi:10.1111/j.1365-2958.2008.06557.x
First published online 11 December 2008

Alcohol oxidase (AOX1) from *Pichia pastoris* is a novel inhibitor of prion propagation and a potential ATPase

Hong Zhang,[1,2] Harriët M. Loovers,[3] Li-Qiong Xu,[1,2] Mingzhu Wang,[1,2] Pamela J. E. Rowling,[4] Laura S. Itzhaki,[4] Weimin Gong,[1] Jun-Mei Zhou,[1] Gary W. Jones[3] and Sarah Perrett[1]*

[1]*National Laboratory of Biomacromolecules, Institute of Biophysics, Chinese Academy of Sciences, 15 Datun Road, Chaoyang District, Beijing 100101, China.*
[2]*Graduate School of the Chinese Academy of Sciences, Beijing 100039, China.*
[3]*Department of Biology, National University of Ireland Maynooth, Maynooth, Co. Kildare, Ireland.*
[4]*MRC Cancer Cell Unit, Hutchison/MRC Research Centre, Hills Road, Cambridge CB2 0XZ, UK.*

Summary

Previous results suggest that methylotrophic yeasts may contain factors that modulate prion stability. Alcohol oxidase (AOX), a key enzyme in methanol metabolism, is an abundant protein that is specific to methylotrophic yeasts. We examined the effect of *Pichia pastoris* AOX1 on prion phenotypes in *Saccharomyces cerevisiae*. The *S. cerevisiae* prion states [*PSI*$^+$] and [*URE3*] arise from aggregation of the proteins Sup35p and Ure2p respectively, and correlate with the ability of Sup35p and Ure2p to form amyloid-like fibrils *in vitro*. We found that expression of *P. pastoris* AOX1 in *S. cerevisiae* had no effect on propagation of the [*PSI*$^+$] prion, but inhibited propagation of [*URE3*]. Addition of AOX1 early in the time-course of fibril formation inhibits Ure2p fibril formation *in vitro*. AOX1 has not previously been identified as an ATPase. However, we discovered that in addition to its flavin adenine dinucleotide-dependent AOX activity, AOX1 possesses ATPase activity. This study identifies AOX1 as a novel prion inhibitory factor and a potential ATPase.

Introduction

Alcohol oxidase (AOX; EC 1.1.3.13), which belongs to the family of glucose–methanol–choline oxidoreductases (Kiess *et al*., 1998), catalyses oxidation of short aliphatic alcohols, such as methanol, ethanol and 1-propanol (Kato *et al*., 1976). The enzyme is found mainly in the peroxisome matrix of methylotrophic yeasts (Lee and Komagata, 1983) and is also found in some other fungi (Janssen *et al*., 1965; Danneel *et al*., 1994; Holzmann *et al*., 2002; Ko *et al*., 2005; Kondo *et al*., 2008). AOX is a key enzyme in methanol metabolism and catalyses the first step in methanol catabolism – oxidation of methanol to formaldehyde with concomitant production of H_2O_2 (reviewed in Ozimek *et al*., 2005). In methylotrophic yeasts, AOX is an abundant protein and its synthesis is strictly regulated at the transcriptional level by methanol induction (Roggenkamp *et al*., 1984; Sibirny *et al*., 1987).

There are a number of different AOX isozymes that are adapted to different environmental methanol concentrations (Ito *et al*., 2007). The number and type of AOX isozymes present in different methylotrophic yeasts vary between species. *Pichia methanolica* has nine AOX isozymes (Gruzman *et al*., 1996), whereas only two AOX isozymes, AOX1 and AOX2, have been found in *Pichia pastoris* (Cregg *et al*., 1989). Although AOX1 and AOX2 share 97% identity in amino acid sequence, expression of AOX1 and AOX2 in *P. pastoris* is controlled by different promoters (Cregg *et al*., 1989). AOX1 constitutes the majority of AOX protein in the cell and is the main contributor to methanol metabolism: growth of an AOX1-defective strain is very slow in methanol media, whereas a defect in AOX2 has little effect on growth (Cregg *et al*., 1989).

The mature active form of AOX is an oligomer: AOX in some methylotrophic yeast species is a molecule of high molecular mass (600 kDa), reported to consist of eight identical subunits, each of which carries one non-covalently bound flavin adenine dinucleotide (FAD) molecule as the prosthetic group (Roa and Blobel, 1983; Goodman *et al*., 1984; Evers *et al*., 1995), although tetrameric (Bystrykh *et al*., 1989) and hexameric (Hopkins, 1986; Kondo *et al*., 2008) forms of AOX have also been reported. FAD binding and assembly of the AOX oligomer are necessary steps in AOX biosynthesis (Evers *et al*., 1996; Ozimek *et al*., 2003). The 3-D structure of AOX has not yet been solved. However, models of the three major domains (FAD-binding domain, flavin attachment loop and substrate-binding domain) and two minor domains

Accepted 17 November, 2008. *For correspondence. E-mail sarah.perrett@iname.com; Tel. (+86) 10 6485 6727; Fax (+86) 10 6487 2026.

(FAD-covering loop and extended FAD-binding domain) have been predicted by structural alignment of AOX with other proteins of the glucose–methanol–choline oxidoreductase family (Kiess *et al*., 1998). The most conserved region is the FAD-binding domain, which comprises four sequence regions distributed over the whole primary sequence. The first region is an ADP-binding motif (βαβ) common to most FAD-binding proteins, and includes the characteristic nucleotide-binding site GXGXXG. In the case of AOX1, the nucleotide-binding site (GGGSSG) is formed by residues 13–18 of the amino acid sequence (Kiess *et al*., 1998).

When peroxisomes were purified from the methylotrophic yeast *Hansenula polymorpha* grown in methanol, it was found that peroxisomal peak fractions which showed AOX and catalase activity also showed ATPase activity (Douma *et al*., 1987). The observed ATPase activity is Mg^{2+}-dependent and has a pH optimum of approximately 8.5 (Douma *et al*., 1987). Although some ATPases in the membrane of the peroxisome have since been discovered (Douma *et al*., 1990; Titorenko and Rachubinski, 2000), the relationship between the observed ATPase activity and the presence of AOX in the peroxisome matrix remains unclear.

Ure2p is the corresponding yeast prion protein of the epigenetic factor [*URE3*] (Wickner, 1994), and is a good model for studying the prion phenomenon (Perrett and Jones, 2008). The 354-amino-acid homodimeric protein Ure2p regulates nitrogen metabolism in *Saccharomyces cerevisiae* (Coffman *et al*., 1994). On conversion to the [*URE3*] prion state Ure2p changes its conformation, forms aggregates, and loses its normal function in control of nitrogen metabolism (Masison and Wickner, 1995). *In vitro*, Ure2p forms fibrillar amyloid-like aggregates (Taylor *et al*., 1999; Thual *et al*., 1999). Ure2p consists of a relatively flexible and protease-sensitive N-terminal region (~90 amino acids), and a globular C-terminal region (Perrett *et al*., 1999; Thual *et al*., 1999). The N-terminal region is essential for its prion properties *in vivo* and to form amyloid-like filaments *in vitro* (Taylor *et al*., 1999; Thual *et al*., 2001). However, stability or folding of the protein *in vitro* is not affected by deletion of the N-terminal region (Perrett *et al*., 1999; Galani *et al*., 2002). The crystal structure shows that the C-terminal region shares structural similarity with glutathione transferases (GSTs) (Bousset *et al*., 2001; Umland *et al*., 2001). The C-terminal region is responsible for the regulatory function of Ure2p *in vivo* (Coschigano and Magasanik, 1991; Masison and Wickner, 1995) and also for its glutathione-dependent peroxidase (GPx) activity (Rai *et al*., 2003; Bai *et al*., 2004); point mutation in the C-domain of Ure2p is sufficient to allow reaction with typical GST substrates (Zhang *et al*., 2008). The GPx (or GST) activity of Ure2p (or its point mutants) is maintained upon formation of fibrillar aggregates, indicating that the native structure of the C-terminal region is retained within the fibrils (Bai *et al*., 2004; Zhang *et al*., 2008).

[*URE3*] and [*PSI*$^+$] (whose corresponding yeast prion protein is Sup35p) in *S. cerevisiae* were the first two yeast prions discovered (Wickner *et al*., 1995). The prion phenomenon has since been found in a number of different fungal species, but has not so far been studied in methylotrophic yeasts. Nevertheless, the prion domain of *P. methanolica* Sup35p was found to convey prion properties when expressed in *S. cerevisiae*, although both induction and loss of the prion state occurred more readily for the *Pichia* than the *S. cerevisiae* sequence (Chernoff *et al*., 2000; Kushnirov *et al*., 2000; Zadorskii *et al*., 2000). These results suggest that prions exist in methylotrophic yeasts, but that species-specific factors may contribute to the stability of both native and prion forms of the protein. AOX is an abundant and specific protein in methylotrophic yeasts. We tested the effect of *P. pastoris* AOX1 on prion propagation in *S. cerevisiae*. Interestingly, overexpression of AOX1 specifically inhibited [*URE3*] propagation *in vivo* and the presence of AOX1 inhibited Ure2p amyloid fibril formation *in vitro*. We also found that in addition to its FAD-dependent AOX activity, AOX1 possesses ATPase activity.

Results

*Overexpression of AOX1 impaired [*URE3*] propagation*

Proteins homologous to the yeast prion protein Sup35p have been identified in methylotrophic yeasts, and *P. methanolica* Sup35p shows prion properties when expressed in *S. cerevisiae* (Chernoff *et al*., 2000; Kushnirov *et al*., 2000; Zadorskii *et al*., 2000). However, the results suggest involvement of species-specific factors in both stabilization against prion induction and reliable propagation of the prion state (Chernoff *et al*., 2000; Kushnirov *et al*., 2000). AOX is a highly abundant protein that is unique to methylotrophic yeasts. We tested whether overexpression of *AOX1* had effects on prion propagation in *S. cerevisiae*.

AOX1 was placed under control of the strong promoter of *SSA2*, a cytosolic Hsp70 homologue known to modulate prion propagation (Roberts *et al*., 2004; Loovers *et al*., 2007) that has a similar monomeric molecular weight to AOX1. We found that overexpression of *AOX1* had no effect on [*PSI*$^+$] propagation, related to the Sup35 protein (data not shown), but impaired [*URE3*] propagation, related to the Ure2 protein. Figure 1 and Table 1 show the effect of overexpression of *AOX1* on [*URE3*] propagation, compared with the vector control. Using the SB34 strain allows for assessment of [*URE3*] status by colour assay. Soluble functional Ure2p prevents induction

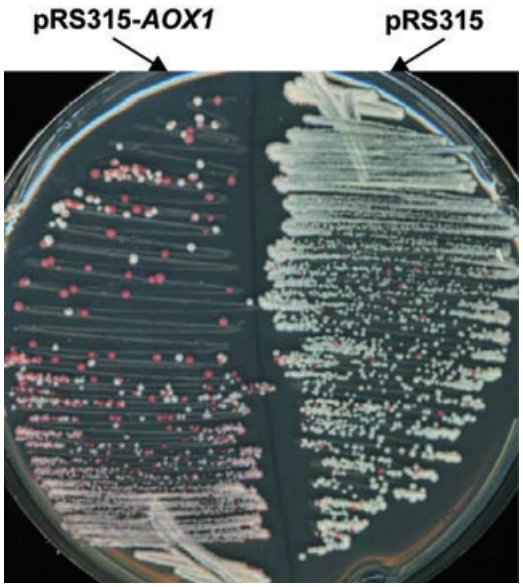

Fig. 1. [*URE3*] phenotype of yeast cells overexpressing *AOX1* under control of the *SSA2* promoter. Cells were streaked onto YPD and incubated at 30°C for 2 days followed by a further 2 days at room temperature. White colour is indicative of the presence of the [*URE3*] prion; pink and red colonies reflect a reduction in expression of the *ADE2* reporter gene and [*ure0*] cells respectively.

of the *DAL5* promoter by binding to the transcription factor Gln3p. Hence the downstream *ADE2* gene is not expressed and the accumulation of an intermediate in the purine biosynthesis pathway, which is the substrate of Ade2p, leads to red-pigmented cells (Silver and Eaton, 1969). When Ure2p is in the [*URE3*] prion state, functional binding to Gln3p is lost, allowing expression of *ADE2* under *DAL5* control. The red pigment is metabolized by Ade2p and so no longer accumulates, hence [*URE3*] cells are white. The presence of overexpressed *AOX1* had a clear effect on [*URE3*] propagation, as is reflected by the appearance of red and pink colonies. These results raise the possibility that AOX1 acts as a specific anti-prion factor towards [*URE3*], and pose the question whether the curing effect we observed for AOX1 is related to a direct interaction between AOX1 and Ure2p.

Pure AOX1 was obtained from P. pastoris *by a three-step purification*

AOX1 is essential to allow yeast to utilize methanol as a carbon source (Patel *et al*., 1981). When *P. pastoris* cells are grown in methanol media (without any other carbon source), the amount of AOX protein can reach 20–30% of the total cellular protein (Veenhuis *et al*., 1983). During the process of purification by anion exchange, ammonium sulphate precipitation and size exclusion chromatography (SEC), SDS-PAGE stained with Coomassie brilliant blue showed a band at around 75 kDa that was increasingly pure with each step (data not shown). After the last step, only one band at around 75 kDa could be seen on the SDS gel (Fig. 2A). The purified protein also showed only one band on native-PAGE (Fig. 2B) and only a single peak eluted from a 24 ml SEC column (Fig. 2C). The position of AOX1 on both native-PAGE and SEC was close to the 443 kDa protein standard, and the calculated molecular weight of AOX1 was 414 ± 14 kDa according to the SEC standard curve (see *Experimental procedures*). According to the sedimentation coefficient determined by analytical ultracentrifugation, the estimated molecular mass of AOX1 was 546 ± 44 kDa (Table 2). The purified protein appeared as uniform globular particles with diameter of around 20 nm by electron microscopy (Fig. 2D). All of the above indicated that our purified protein was a homogeneous oligomer, corresponding to a hexamer or octamer. AOX purchased from Sigma appeared the same as purified AOX1 by SDS-PAGE, Western blot (data not shown), SEC, and velocity sedimentation (Table 2). The purified protein (at around 100 μM concentration) appears golden yellow consistent with the presence of an FAD prosthetic group.

N-terminal sequencing showed that the first 10 amino acids of the purified protein were 'AIPEE FDILV'. Blasting this 10-amino-acid sequence in the NCBI or Expasy databases identified it as an AOX isozyme. Matrix assisted laser desorption/ionization time-of-flight mass spectrometry (MALDI-TOF MS) analysis (followed by searching in the NCBInr database) of trypsin-digested AOX1 indicated a closer match to AOX1 than to AOX2. We therefore

Table 1. Effect of *AOX1* overexpression on [*URE3*] propagation.

Plasmid	% white colonies	% red colonies	% sectored colonies	Colour after re-streak[a]
pRS315 (vector control)	95	1	4	1
pRS315-*AOX1* (*SSA2* promoter)	62	10	28	6

Colony percentage is given after transformation of plasmid into SB34 and colour after re-streak is for a colony from [*URE3*] selective medium, as described in *Experimental procedures*.
a. Colony colour was scored subjectively on a scale from 0 to 9; 0 = White = [*URE3*] = 'prion state', 9 = Red = [*ure0*] = 'cured' (Loovers *et al*., 2007).

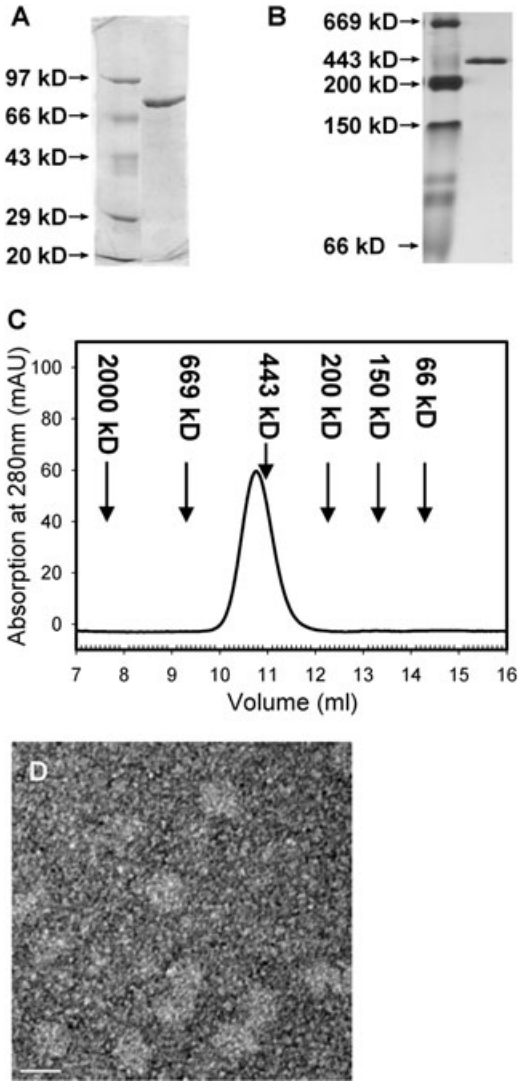

Fig. 2. Characterization of purified AOX1.
A. 10% SDS-PAGE of AOX1, with molecular mass standards as indicated.
B. Gradient native-PAGE (5–15%) of AOX1, with molecular mass standards as indicated.
C. Elution profile of AOX1 SEC, calibrated by blue dextran (2000 kDa, 7.67 ml), thyroglobulin (669 kDa, 9.30 ml), apoferritin (443 kDa, 10.96 ml), β-amylase (200 kDa, 12.29 ml), alcohol dehydrogenase (150 kDa, 13.21 ml), and bovine serum albumin (66 kDa, 14.21 ml). The position of the AOX1 peak was 10.77 ml. The molecular weight of AOX1 calculated from the resulting standard curve was 414 ± 14 kDa.
D. Electron microscope image of AOX1, the bar represents 20 nm.

concluded that our purified protein was a homogenous preparation of *P. pastoris* AOX1.

When the AOX activity towards methanol of the purified AOX1 and AOX purchased from Sigma was compared, similar K_M and k_{cat} values were obtained for the two different sources of AOX, as shown in Table 3. (In both cases, the observed level of activity was dependent on the solution conditions and was higher in phosphate buffer than in Tris buffer, Table 3.) This indicates that the purified AOX1 was functional and showed the expected enzyme activity.

ATPase activity of AOX1

ATPase activity of AOX1 has not been reported previously. However, we unexpectedly discovered that AOX1 has the ability to promote ATP hydrolysis. In a coupled enzymatic assay (see *ATPase assay I* in *Experimental procedures*), the velocity of NADH consumption indicated that the velocity of ADP generation was linearly related to the amount of AOX1 protein present in the ATPase assay system (Fig. 3A). When different concentrations of the substrate ATP were used, we observed typical Michaelis–Menten plots (Fig. 3B), from which a K_M of 140 ± 14 μM and V_{max} of 16.2 ± 0.6 nmol min^{-1} mg^{-1} was obtained by fitting to the equation: $y = V_{max} * x/(K_M + x)$, where y is the

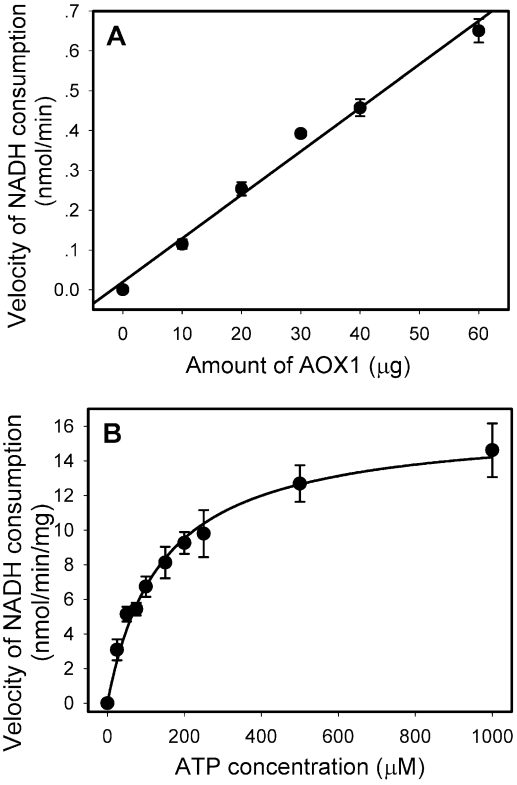

Fig. 3. ATPase activity of AOX1 detected by coupled-enzyme assay. ATPase assay of AOX1 was performed at 30°C in 50 mM Tris-HCl buffer, pH 7.5, containing 200 mM KCl, 10 mM $MgCl_2$, 1 mM DTT and 2.5% glycerol for 400 s. NADH consumption was monitored to detect generation of ADP by AOX1-catalysed ATP hydrolysis. The data shown are the mean of three individual samples and the error bars represent the standard error of the mean.
A. Velocity of ATP hydrolysis against AOX1 protein concentration.
B. Michaelis–Menten plots showing variation of AOX1 ATPase activity with substrate concentration. The fit shown gives values for K_M of 140 ± 14 μM and for V_{max} of 16.2 ± 0.6 nmol min^{-1} mg^{-1}.

Table 2. Determination of oligomeric state of AOX.

	Calculated monomeric molecular mass (kDa)	Determination of oligomeric state of AOX by different techniques				
		SEC[a]		Velocity sedimentation		
		Peak position (ml)	M_{app} (kDa)	Sedimentation coefficient (S)	M_{app} (kDa)	Oligomeric state
Purified AOX1 in Tris buffer with DTT	73.9	10.77	414 ± 14	ND	ND	Hexamer or octamer
Sigma AOX in Tris buffer with DTT	73.9	10.68	433 ± 15	ND	ND	Hexamer or octamer
Purified AOX1 in Tris buffer without DTT	73.9	10.56	458 ± 15	Monodisperse $S_{20,w}$ = 19.3 ± 1.0	546 ± 44	Hexamer or octamer
Purified AOX1 in phosphate buffer without DTT	73.9	10.60	449 ± 15	Monodisperse $S_{20,w}$ = 19.3 ± 1.2	548 ± 47	Hexamer or octamer
Sigma AOX in phosphate buffer without DTT	73.9	10.59	451 ± 15	Monodisperse $S_{20,w}$ = 19.3 ± 0.8	540 ± 39	Hexamer or octamer

a. A Superdex 200 10/300 GL column (Amersham Biosciences) was used.

velocity of NADH consumption and *x* is the ATP concentration. Although the coupled enzymatic assay should reflect ADP generation, we found in controls that AOX1 can also promote dephosphorylation of phosphoenolpyruvate (PEP), which is directly related to NADH consumption in the assay system. We therefore added ATP to initiate the catalysed ATP hydrolysis reaction after first obtaining a 200 s baseline. Thus the interference from catalysed dephosphorylation of PEP could be subtracted by using the difference in slope between the 200 s initial baseline and the 400 s measurement to represent the rate of ATP hydrolysis.

In order to use an additional method to confirm the ability of AOX1 to catalyse ATP hydrolysis, and to avoid the complication of the coupled enzymatic assay system described above, we also measured release of inorganic phosphate using malachite green (see *ATPase assay II* in *Experimental procedures*). We found that the accumulation of inorganic phosphate was almost linear with the reaction time (Fig. 4A) and depended linearly on the amount of AOX1 protein (Fig. 4B). Michaelis–Menten plots were fitted as above (Fig. 4C), giving a K_M of 354 ± 26 μM and V_{max} of 2.5 ± 0.1 nmol min^{-1} mg^{-1}. The difference in the kinetic parameters obtained by different ATPase assay methods is a commonly observed phenomenon and is related to the different reaction times used in the two methods (i.e. the first 400 s of the reaction was monitored in the coupled enzymatic assay, so the velocity was near to the initial velocity; whereas we monitored the reaction for around 10 h for inorganic phosphate determination, so the velocity represents the average velocity over an extended time period).

In order to further confirm that the observed ATPase activity is due to the AOX1 protein itself, and not due to any contaminant, we crystallized the AOX1 protein and then recovered the protein crystals for analysis (see *Experimental procedures*). It has been reported previously that the AOX1 protein crystallizes extremely readily, although no crystal structure is yet available as the crystals diffract only poorly (Boys *et al.*, 1989; Van der Klei *et al.*, 1989; Veenhuis *et al.*, 1981). Under the range of conditions used here (see *Experimental procedures*), crystals appeared within 24 h (Fig. 5A), and remained stable in the crystallization buffer for at least one year. The crystallized AOX1 protein was recovered, rinsed in fresh crystallization buffer, and then resuspended in the activity assay buffer for further analysis. The identity of the crystallized protein was confirmed to be AOX1 by SDS-PAGE (Fig. 5B), and by subjection of the trypsin-digested sample to MALDI-TOF MS, as described above. As

Table 3. Alcohol oxidase activity of AOX1 using methanol as substrate.

	Phosphate buffer[a]		Tris buffer[b]	
	K_M (mM)	k_{cat} (s^{-1})	K_M (mM)	k_{cat} (s^{-1})
Purified AOX1	0.73 ± 0.24	2.96 ± 0.25	2.35 ± 0.18	1.45 ± 0.04
Sigma AOX	0.61 ± 0.06	4.41 ± 0.09	1.10 ± 0.30	1.04 ± 0.08

AOX protein purchased from Sigma is used as a comparison.
a. 50 mM sodium phosphate buffer, pH 7.5.
b. 50 mM Tris-HCl buffer, pH 7.5, containing 200 mM KCl and 10 mM $MgCl_2$.

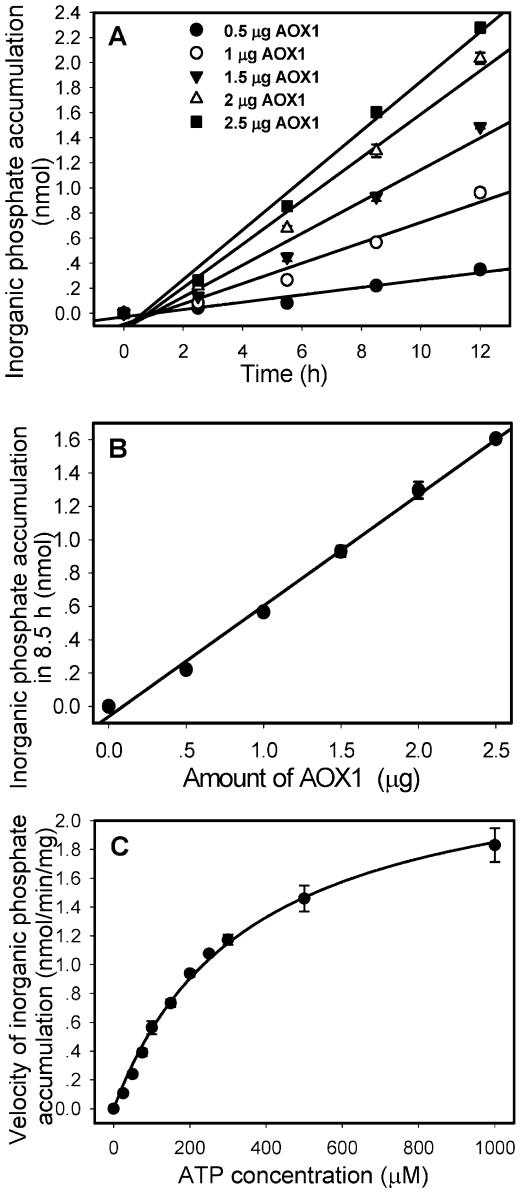

Fig. 4. ATPase activity of AOX1 detected by inorganic phosphate determination with malachite green. ATPase assay of AOX1 was performed at 30°C in 50 mM Tris-HCl buffer, pH 7.5, containing 50 mM KCl, 10 mM $MgCl_2$ and 2 mM DTT. The data shown are the mean of three individual samples and the error bars represent the standard error of the mean.
A. Inorganic phosphate produced by ATP hydrolysis catalysed by different amounts of AOX1.
B. Data from (A) plotted as ATPase activity against AOX1 protein concentration for the 8.5 h time point.
C. Michaelis–Menten plots showing variation of AOX1 ATPase activity with substrate concentration, monitored for 11 h. The fit shown gives values for K_M of 354 ± 26 μM and for V_{max} of 2.5 ± 0.1 nmol min^{-1} mg^{-1}.

shown in Fig. 5C, the crystallized protein showed ATPase activity, as monitored by the malachite green assay. This confirms that a highly pure and homogenous preparation of AOX1 protein shows ATPase activity.

We found that magnesium is essential for the ATPase activity of AOX1, with 5 mM magnesium being sufficient for activity measurements (Fig. 6A). Dithiothreitol (DTT) was also essential for ATPase activity of AOX1 (data not shown). The concentration of potassium and sodium did not affect the ATPase activity of AOX1, and the enzyme

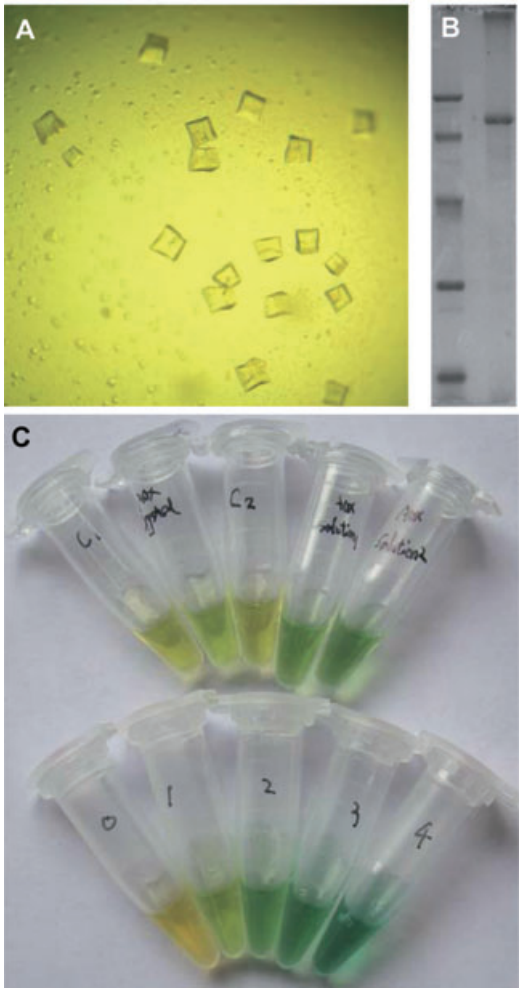

Fig. 5. ATPase activity of crystallized AOX1 detected by inorganic phosphate determination with malachite green.
A. Typical AOX1 crystals observed under the polarizing microscope. The crystals shown were grown in a 1:5 v/v tert-butanol : water mixture. Crystals were removed from the crystallization liquor, rinsed with fresh crystallization solution and resuspended in SDS-PAGE loading buffer or the activity assay buffer.
B. 10% SDS-PAGE of recovered crystals of AOX1 (right lane) with molecular mass standards (left lane; standards were as indicated in Fig. 2A).
C. ATPase assay of recovered crystals of AOX1 was performed at 30°C in 50 mM Tris-HCl buffer, pH 7.5, containing 10 mM $MgCl_2$ and 2 mM DTT, for 12 h, using the malachite green reagent (see *Experimental procedures*). Upper set of tubes, left to right: control without AOX1, crystallized AOX1, control without AOX1 (replicate), AOX1 solution before crystallization, AOX1 solution before crystallization (replicate). Lower set of tubes, left to right: 0, 1, 2, 3 and 4 nmol inorganic phosphate standards.

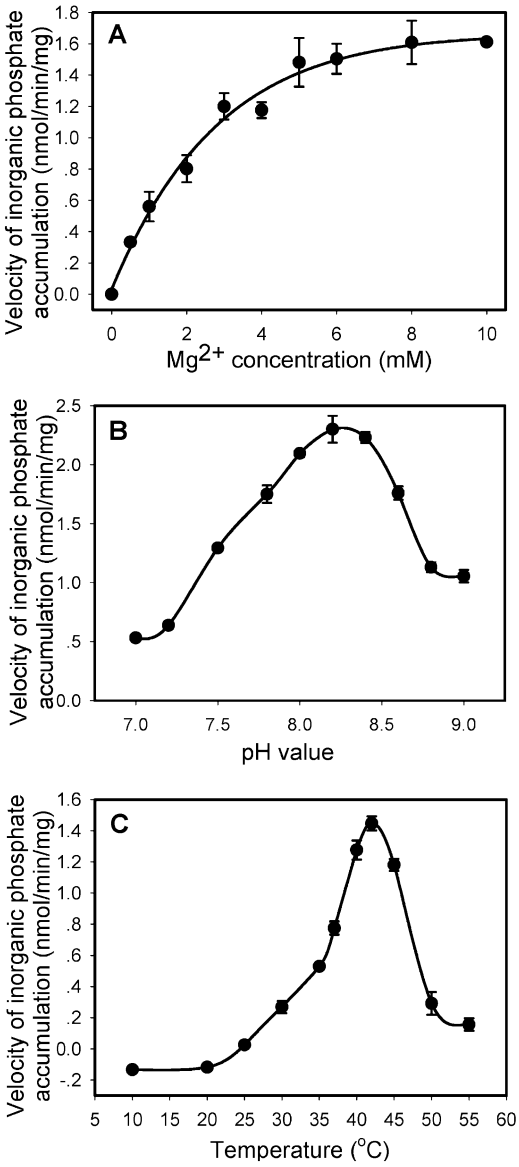

Fig. 6. Optimum conditions for ATPase activity of AOX1. The data shown are the mean of three individual samples and the error bars represent the standard error of the mean.
A. Effect of Mg^{2+} concentration on ATPase activity of AOX1. ATPase assay of AOX1 was performed at 30°C in 50 mM Tris-HCl buffer, pH 7.5, containing 50 mM KCl, 2 mM DTT and different concentrations of $MgCl_2$, for 9 h.
B. The pH optimum of ATPase activity of AOX1. ATPase assay of AOX1 was performed at 30°C in 50 mM Tris-HCl buffers of different pH value (as indicated), containing 50 mM KCl, 10 mM $MgCl_2$ and 2 mM DTT for 11 h.
C. Temperature optimum of ATPase activity of AOX1. ATPase assay of AOX1 was performed in 40 mM HEPES buffer, pH 7.5, containing 50 mM KCl, 10 mM $MgCl_2$ and 2 mM DTT for 11 h at different temperatures, as indicated.

activity remained unchanged in the absence of these two ions (data not shown). We found that the observed ATPase activity of AOX1 was sensitive to the buffer conditions: the activity in Tris buffer was higher than that in HEPES buffer, and in phosphate buffer no activity could be detected (data not shown).

To obtain the pH optimum, Tris buffer was employed. We found the optimum pH for the AOX1 ATPase was pH 8.2 (Fig. 6B). To obtain the temperature optimum, HEPES buffer was used, because the pH of Tris buffer varies with temperature. We found the optimum temperature for the AOX1 ATPase activity was 42°C (Fig. 6C). The optimum pH and optimum temperature of AOX1 ATPase activity are similar to those reported for its AOX activity (Hopkins, 1986). The ATPase activity of AOX1 remained unchanged for 2 weeks at 4°C in Tris buffer (data not shown), which indicates similar stability to that reported for its AOX activity (Hopkins, 1986). However, after prolonged storage in phosphate buffer followed by transfer to Tris buffer, ATPase activity could no longer be detected (although AOX activity was maintained), which explains why no ATPase activity could be detected in AOX purchased from Sigma (which is supplied in phosphate buffer). This resembles the case of phage T4 polynucleotide kinase, where the observed activity in phosphate buffer is only 5% of that in Tris buffer (Sambrook *et al.*, 1989). The far-UV circular dichroism and intrinsic fluorescence spectra of the AOX1 protein remained unchanged after incubation under these different conditions (data not shown), and no degradation was detected by SDS-PAGE, ruling out any significant change in overall secondary structure of the protein accompanying the observed changes in enzymatic activity.

The presence of AOX1 inhibits amyloid-like fibril formation of Ure2p

Ure2p forms amyloid-like fibrils *in vitro* (Taylor *et al.*, 1999; Thual *et al.*, 1999) and binding of the fluorescence dye thioflavin T (ThT) is a convenient method to follow the time-course of formation of amyloid-like structure (Naiki *et al.*, 1989; Nielsen *et al.*, 2001). In the case of Ure2p, increased ThT fluorescence correlates directly with formation of fibrillar aggregates, as observed by atomic force microscopy (AFM) (Jiang *et al.*, 2004). We therefore used a combination of these methods to monitor the effect of various concentrations of AOX1 on the fibril formation kinetics of Ure2p.

We found that the presence of AOX1 reduced the amount of fibrillar aggregates formed in a concentration-dependent manner as observed by AFM (Fig. 7A–E) and ThT binding (Fig. 7F and G). A ratio as low as 1:30 of AOX1 : Ure2p was sufficient to observe an effect on fibril formation of Ure2p (Fig. 7F). When the molar concentration of AOX1 was equal to or exceeded that of Ure2p, the fibril formation of Ure2p was strongly inhibited (Fig. 7D and G). The inhibitory effect of AOX1 on Ure2p fibril formation was similar at the yeast growth temperature of

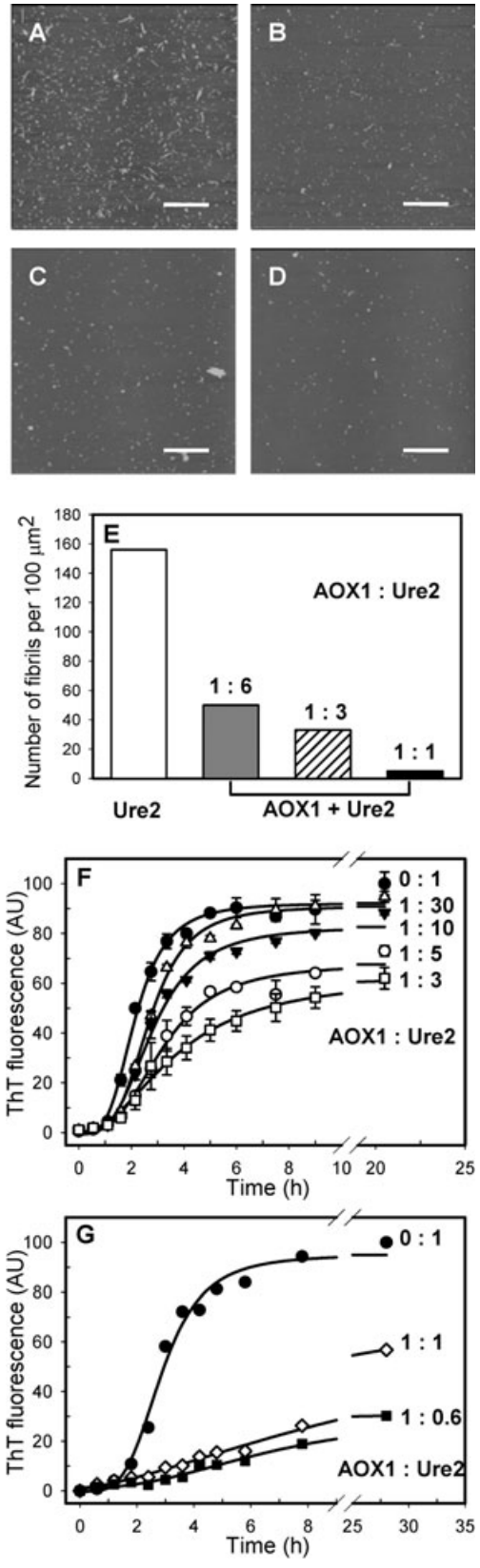

Fig. 7. AOX1 concentration-dependent inhibition of Ure2p fibril formation. Fibril formation of Ure2p in the presence of different concentrations of AOX1 was performed at 30°C in 50 mM Tris-HCl buffer, pH 7.5, containing 150 mM NaCl, 50 mM KCl, 10 mM $MgCl_2$, 1 mM DTT, 0.625% glycerol and 0.02% NaN_3 with shaking.
10 μm × 10 μm square scan areas were randomly taken from 8th hour (i.e. plateau phase) samples for analysis by AFM. Representative scan areas are shown for 30 μM Ure2p alone (A) and in the presence of 5 μM (B), 10 μM (C) or 30 μM (D) AOX1 (the bars represent 2 μm).
E. The number of fibrils in each of the AFM scan areas shown was calculated manually.
F. The time-course of fibril formation of 36 μM Ure2p in the presence of 0 μM (●), 1.2 μM (△), 3.6 μM (▼), 7.2 μM (○) and 11.5 μM (□) AOX1 was monitored by ThT-binding fluorescence. The data shown are the mean of three replicate samples and the error bars represent the standard error of the mean.
G. The time-course of fibril formation of 30 μM Ure2p in the presence of 0 μM (●), 30 μM (◇) and 45 μM (■) AOX1 was monitored by ThT-binding fluorescence.

30°C (Fig. 7) and at 10°C (data not shown). The presence of ADP (data not shown) or ATP (Fig. 8C) had negligible effect on the inhibitory effect of AOX1 on Ure2p fibril formation. The above results are consistent with stoichiometric interaction between AOX1 and Ure2p, leading to inhibition of formation of amyloid-like structure, which is consistent with the curing effect of AOX1 overexpression on [*URE3*] propagation *in vivo* (Fig. 1).

Under the same conditions, equimolar Sigma AOX also showed an inhibitory effect on Ure2p fibril formation monitored by ThT binding (data not shown). As controls, the presence of an equimolar concentration of bovine serum albumin (BSA) had no inhibitory effect on the time-course of Ure2p fibril formation (data not shown), indicating that the inhibitory effect of AOX1 is specific. AOX1 incubated alone under the conditions of the experiment showed no ThT fluorescence and no fibrillar structures were formed (data not shown).

To investigate at what stage in the Ure2p fibril formation process inhibition by AOX1 is effective, we investigated the effect of delaying the addition of AOX1. We found that AOX1 was still effective when added mid-way through the lag phase of Ure2p fibril formation (Fig. 8A and C), but had no effect when added in early or late exponential phase (Fig. 8B and C). This was true in the absence of nucleotide (Fig. 8A and B) and in the presence of ATP (Fig. 8C). From this we can conclude that AOX1 inhibits Ure2p fibril formation by interaction with a species present during the very early stages of the fibril formation process.

Discussion

Yeast prions are good models for understanding the molecular mechanism of the aggregation process underlying amyloid diseases, including the prion diseases (Shorter and Lindquist, 2005; Wickner *et al.*, 2007; Perrett and Jones, 2008). Inhibitory factors, including molecular

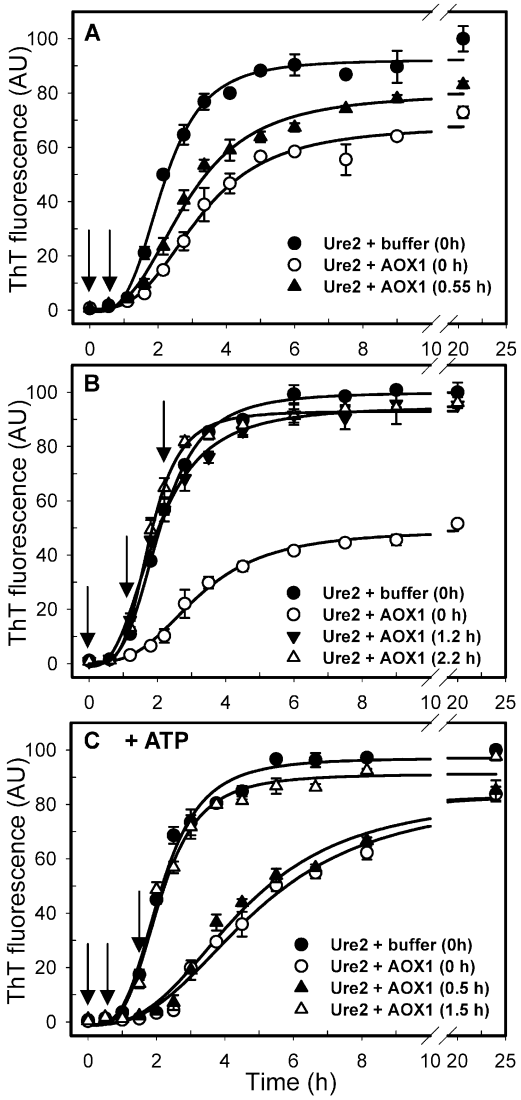

Fig. 8. Effect of delayed addition of AOX1 on inhibition of Ure2p fibril formation. Fibril formation of 36 μM Ure2p was performed under the same conditions as described in the legend to Fig. 7 and was monitored by ThT-binding fluorescence. AOX1 (or an equivalent volume of buffer) was added at different time intervals to give a ratio of AOX1 : Ure2p of 1:5, as indicated. The data shown are the mean of three replicate samples and the error bars represent the standard error of the mean.
A and B. In the absence of nucleotide, 7.2 μM AOX1 was added at 0 h (○), 0.55 h (▲), 1.2 h (▼) or 2.2 h (△). In the control, buffer was added at 0 h (●).
C. In the presence of 1 mM ATP (with an ATP regeneration system), 7.2 μM AOX1 was added at 0 h (○), 0.5 h (▲) and 1.5 h (△). In the control, buffer was added at 0 h (●).

chaperones and anti-amyloid drugs, are widely studied because such research may give clues for prophylaxis and therapy of amyloid diseases (Jones and Tuite, 2005; Tribouillard-Tanvier *et al.*, 2008). Methylotrophic yeasts possess homologues of yeast prion proteins, raising the question whether they also have factors that modulate prion propagation (Chernoff *et al.*, 2000; Kushnirov *et al.*, 2000). AOX, an abundant protein specific to methylotrophic yeasts, is a potential candidate for this type of influencing factor. In this study we showed that AOX1 from *P. pastoris* could impair propagation of the *S. cerevisiae* prion [*URE3*] *in vivo* and amyloid fibril formation of its prion protein Ure2 *in vitro*. Further, we discovered that AOX1 has ATPase activity.

In comparison with the vector control, *AOX1* had a marked effect on [*URE3*] propagation (Fig. 1). Transformation of the same AOX1 plasmid into a [*PSI*$^+$] strain had no effect on [*PSI*$^+$] propagation, suggesting that the anti-prion effect of AOX1 is specific towards [*URE3*]. We blasted the *S. cerevisiae* Ure2p protein sequence in the Expasy database, and found that the Ure2p homologue in methylotrophic yeasts lacks the prion domain present in *S. cerevisiae* Ure2p. However, it remains possible that other prion proteins similar to *S. cerevisiae* Ure2p exist in methylotrophic yeasts, but their sequences have not yet been included in the available databases.

The effect of AOX1 on [*URE3*] propagation appears to be due to direct interaction between AOX1 and Ure2p, as indicated by *in vitro* analysis (Figs 7 and 8). AOX1 inhibited Ure2p fibril formation, suggesting a direct interaction between the two proteins. AOX1 was only effective when added before the exponential growth phase of Ure2p fibril formation (Fig. 8), suggesting that AOX1 interacts with a species of Ure2p present in the early stages of fibril formation, such as an early intermediate in the aggregation process. When the interaction of AOX1 and Ure2p was examined by surface plasmon resonance or SEC under the conditions of the fibril formation experiments, direct interaction between native AOX1 and native Ure2p could not be detected (data not shown). It is therefore possible that AOX1 interacts with a species of Ure2p that is populated only transiently. The presence of nucleotide was not required for the interaction between AOX1 and Ure2p (Fig. 8), and even in the presence of ATP, AOX1 was unable to disaggregate fibrils of Ure2p that had already been formed (Fig. 8), ruling out one possible role of the ATPase activity of AOX1.

ATPase activity of the peroxisomal fraction of methylotrophic yeast cells has been observed and coincides with the location of AOX (Douma *et al.*, 1987). However, AOX1 has never been suspected to be an ATPase, and the presence of a nucleotide-binding motif in the predicted structure (Kiess *et al.*, 1998) is consistent with its established function as an FAD-dependent AOX (Kato *et al.*, 1976). Here, we detected ATPase activity of purified AOX1 by two methods of assay, i.e. by determining production of either ADP or inorganic phosphate, both of which are products of ATP hydrolysis. The ATPase activity of AOX1 is quite weak compared with some other typical ATPases, such as Na^+-K^+-ATPase (Keillor and Jencks, 1996) and Ca^{2+}-ATPase (Bodley and Jencks, 1987), but is

more similar to the ATPase activity of some molecular chaperones, such as Hsp70 (Sadis and Hightower, 1992) and Hsp90 (Rowlands *et al.*, 2004). Similar to the ATPase activity of the whole peroxisome, the ATPase activity of AOX1 is Mg^{2+} dependent and reaches a peak at pH 8.2. However, the k_{cat} of AOX1 ATPase represents only 1% of the whole peroxisome ATPase activity. Further, the K_M of AOX1 ATPase is below 0.5 mM ATP but the K_M of the whole peroxisome ATPase activity is 4–6 mM ATP (Douma *et al.*, 1987). The ATPase activity of AOX1 is also strictly sulfhydryl reducer-dependent like some other enzymes containing cysteines. Na^+ and K^+ are not necessary for the ATPase activity, unlike the ATPase activity of some molecular chaperones (Lopez-Buesa *et al.*, 1998; Boero *et al.*, 2006). The similar optimum pH, optimum temperature and stability of the ATPase and AOX activities of AOX1 (see Fig. 6B and C and Hopkins, 1986) suggest one protein with two different enzyme activities.

Although AOX1 readily crystallizes, the crystals give poor diffraction (Veenhuis *et al.*, 1981; Van der Klei *et al.*, 1989), and so its crystal structure remains unsolved. However, it is apparent that the AOX1 sequence contains the motif $GXGXXG(X)_{17-19}E$ (i.e. GGGSSGSCIAGR LANLDHSLKVGLIEAGE, residues 13–41) which is commonly found in FAD-containing proteins, particularly those of the glutathione reductase structural family (Dym and Eisenberg, 2001). This motif is also found in some non-FAD-containing proteins, and in general, it is thought to bind phosphate- or sulphate-containing ligands (Dym and Eisenberg, 2001). The $GXGXXG(X)_{18}E$ motif is the only identifiable pyrophosphate-binding motif in AOX1 and is assumed to be involved in FAD binding (Kiess *et al.*, 1998). The ATPase activity of AOX1, and also its ability to promote hydrolysis of the high-energy phosphate compound PEP, raises the possibility that ATP/ADP and PEP may also interact with this motif. To our knowledge, ATPase activity in other FAD-containing proteins has not been reported. The observed ATPase activity of AOX1 may simply represent an example of cross-reactivity with an alternative but similar ligand. The buffer specificity of AOX1 ATPase activity, particularly the lack of activity in phosphate buffer, indicates that the ATPase activity of AOX1 may represent only a potential function that is obscured *in vivo*. Therefore, the biological significance of the ATPase activity of AOX1 still needs further exploration.

Many proteins in the cell exhibit more than one function. Here we present a new angle on the functional capabilities of AOX1. AOX1 has ATPase activity under specific conditions, which suggests that its function in the cytosol may be broader than previously thought. The inhibitory effect of AOX1 on prion propagation of Ure2p suggests that AOX1 may act as a prion inhibitory factor in methylotrophic yeasts, and identifies AOX1 as a novel anti-prion agent.

Experimental procedures

Materials

NADH, ATP and ADP were from Roche or Sigma. Lyticase, lactate dehydrogenase (LDH), pyruvate kinase (PK), PEP, horseradish peroxidase (HRP), tetramethylbenzidine (TMB), Tris, HEPES, sodium azide, DTT and ThT were from Sigma. Commercial AOX was purchased from Sigma (A2404) for comparison with purified AOX1. Molecular mass standards for SEC were purchased from Sigma. Media were from Difco. All other reagents were local products of analytical grade. Milli Q water was used throughout. Solutions were prepared volumetrically and the stated pH of buffers is correct at 25°C. The pH of ATP/ADP solutions was adjusted to pH 7.0 with 0.2 N NaOH before addition to the relevant buffer. The *P. pastoris* strain GS115 was purchased from Invitrogen.

Yeast strains, plasmids and genetic methods

Strains used in this study were SB34 (Bach *et al.*, 2003), which is a derivative of CC34 (*MAT**a***, *trp1-1*, *ade2-1*, *leu2-3,112*, *his3-11,15*, *URA2::HIS3*, [*URE3*]) (Fernandez-Bellot *et al.*, 2000) that has the *ERG6* gene replaced with *TRP1* and the *DAL5* coding sequence replaced by *ADE2*; G400-1C (*MAT**a*** *ade2-1 SUQ5 kar1-1 his3 leu2 lys2 trp1 ura3 ssa1::KanMX*, *ssa2::HIS3*, *ssa3::TRP1*, *ssa4::URA3-1f*/ pRDW10 [*PSI*$^+$]) (Jones and Masison, 2003); and G600 (*MATa ade2.1 SUQ5 kar1-1 his3 leu2 trp1 ura3* [*PSI*$^+$]). The plasmid pC210 contains the *SSA1* coding region under control of the *SSA2* promoter that was cloned into a pRS315 (*LEU2*) backbone (Schwimmer and Masison, 2002). The coding region of the *P. pastoris AOX1* gene with flanking NdeI and SphI restriction enzyme sites was amplified by PCR from genomic DNA isolated from strain GS115; primers used to amplify *AOX1* were HML-aoxf 5′-aattataacatATGGCTATCCC CGAAGAG-3′ and HML-aoxr 5′-ttaaataagcatgcTTAGAATC TAGCAAGACC-3′. The *SSA1* coding sequence in pC210 was then removed by NdeI and SphI digestion and similarly digested *AOX1* PCR product was subcloned downstream of the *SSA2* promoter. The integrity of the resulting plasmid, pRS315-AOX1, was confirmed by sequencing. Assessment of the effects of *AOX1* expression on [*PSI*$^+$] and [*URE3*] prion propagation *in vivo* was conducted by transforming strains G600, G400-1C and SB34 with pRS315-AOX1 and assessing the colour (white, red or sectored) of resulting transformants as described previously (Loovers *et al.*, 2007).

Protein purification

AOX1 was expressed and purified using the *P. pastoris* strain GS115. Cells were first grown in MDH (1.34% (w/v) yeast nitrogen base, 2% (w/v) glucose, 0.004% (w/v) L-histidine, 0.00004% (w/v) biotin) to an optical density of 1.0–5.0 at 600 nm. Expression of AOX1 was then induced by a shift to MMH (1.34% (w/v) yeast nitrogen base, 0.5% (v/v) methanol, 0.004% (w/v) L-histidine, 4×10^{-5}% (w/v) biotin) giving an optical density of 1.0 at 600 nm. After 48 h of incubation at 30°C (0.5% (v/v) methanol was supplemented after 24 h), cells were harvested (5000 *g*, 5 min, 4°C) and the cell pellet resuspended and washed with cold water. Cells were lysed

by a combination of lyticase digestion and sonication (in Buffer A: 20 mM HEPES buffer, pH 5.9, containing 10 mM KCl, 5 mM $MgCl_2$, 50 mM NaCl, 5 mM β-mercaptoethanol and 5% glycerol). After centrifugation (30 000 *g*, 30 min, 4°C), the supernatant was subjected to the following chromatographic purification, which was performed on an ÄKTA Purifier (Amersham Biosciences) at 16°C. First, a 20 ml DEAE fast flow column (Amersham Biosciences) was equilibrated with Buffer A. After loading the cell lysate, bound AOX1 was eluted with a linear gradient from 50 mM to 600 mM NaCl in 200 ml. Fractions containing AOX1 were concentrated, 40% ammonium sulphate was added, and the samples were left at 4°C overnight. The supernatant after centrifugation was loaded onto a 120 ml Superdex 200 HiLoad column (Amersham Biosciences) equilibrated with Buffer B (50 mM Tris-HCl buffer, pH 7.5, containing 10 mM $MgCl_2$, 200 mM KCl, 1 mM DTT and 2.5% glycerol). The presence of AOX1 was confirmed by 10% SDS-PAGE after each purification step.

The AOX1 concentration (in terms of monomers) was measured by absorbance at 280 nm using the calculated extinction coefficient (Gill and von Hippel, 1989) of 94 825 M^{-1} cm^{-1}. Similar results were obtained using the Bradford method, with BSA as standard. AOX1 was stored in Buffer B.

Wild-type Ure2p with an N-terminal 6×His-tag was produced and purified under native conditions as described (Perrett *et al*., 1999; Zhu *et al*., 2003). The concentration of Ure2p (in terms of monomers) was measured by absorbance at 280 nm using the calculated extinction coefficient of 48 200 M^{-1} cm^{-1} (Perrett *et al*., 1999). Ure2p was stored in Buffer C (50 mM Tris-HCl buffer, pH 7.5, containing 200 mM NaCl). All proteins were stored at –80°C and defrosted in a 25°C water bath immediately prior to use.

Characterization of AOX1

The oligomeric state of native AOX1 was estimated by gradient native-PAGE (5–15% gradient Tris glycine gel), SEC (Superdex 200 10/300 GL column, Amersham Biosciences) and velocity sedimentation (45 400 *g*, 4 h). Blue dextran (2000 kDa), thyroglobulin (669 kDa), apoferritin (443 kDa), β-amylase (200 kDa), alcohol dehydrogenase (150 kDa) and BSA (66 kDa) were used as molecular mass standards.

Assay of AOX activity

Assay of AOX activity was performed by using HRP and its substrate TMB to measure the production of H_2O_2. Oxidation of methanol in 20 µl of Buffer B (without DTT or glycerol) or 50 mM phosphate sodium/potassium buffer, pH 7.5 was catalysed by AOX1 for 2 min at 30°C and then 250 ng ml^{-1} HRP and 250 µg ml^{-1} TMB in 180 µl of 0.2 M NaAc buffer (pH 4.0) was added to terminate the reaction (AOX1 is inactive at pH 4.0). TMB when oxidized by H_2O_2 is blue ($\varepsilon_{652\,nm}$ = 39 000 M^{-1} cm^{-1}) and the colour develops fully after 2 h at 37°C under the conditions used here. $V = (A_{652\,nm}/t)/\varepsilon_{652\,nm}$. AOX purchased from Sigma was used as a comparison.

ATPase assay I

ATPase activity was measured using a coupled enzymatic assay, where the consumption of NADH was monitored by the absorbance at 340 nm, as described (Ferard *et al*., 1975). ATPase activity of AOX1 was assayed in Buffer B with 2 U ml^{-1} PK, 10 U ml^{-1} LDH and 4 mM PEP. Unless otherwise stated, the ATP concentration was 500 µM and the AOX1 concentration was 40 µg ml^{-1}. The assays were carried out in thermostatted 1 ml cuvettes at 30°C using a Shimadzu UV-2501 spectrophotometer. Before 0.2 mM NADH (final concentration) was added, the spectrometer was zeroed at 340 nm. After addition of NADH, its oxidation was measured by monitoring the absorbance at 340 nm, for 200 s before ATP was added and for another 400 s after ATP was added. The difference in slope between the 200 s initial baseline and the 400 s measurement represents the rate of ATP hydrolysis. The actual rate of ATP hydrolysis catalysed by AOX1 was obtained by subtracting the rate of ATP self-hydrolysis (i.e. measured in the absence of AOX1). $V = (dA_{340\,nm}/dt)/\varepsilon_{340\,nm}$, where the molar absorbance coefficient for NADH $\varepsilon_{340\,nm}$ = 6200 M^{-1} cm^{-1}.

ATPase assay II

Colorimetric determination of inorganic phosphate produced by ATP hydrolysis was performed using the malachite green reagent, prepared as described (Rowlands *et al*., 2004). Standard conditions for the AOX1 ATPase assay were 50 mM Tris-HCl buffer, pH 7.5, containing 50 mM KCl, 10 mM $MgCl_2$ and 2 mM DTT at 30°C using a 40 µl reaction volume. Unless otherwise stated, the ATP concentration was 1 mM and the AOX1 concentration was 50 µg ml^{-1}. The effect of Mg^{2+} concentration was measured at 30°C in 50 mM Tris-HCl buffer, pH 7.5, containing 50 mM KCl, 2 mM DTT and different concentrations of $MgCl_2$. The pH optimum was measured at 30°C in 50 mM Tris-HCl buffers of different pH value, containing 50 mM KCl, 10 mM $MgCl_2$ and 2 mM DTT. The temperature optimum was measured in 40 mM HEPES buffer, pH 7.5, containing 50 mM KCl, 10 mM $MgCl_2$ and 2 mM DTT at different temperatures. In each case the AOX1-catalysed reaction was allowed to proceed for 9–11 h before quenching the reaction by addition of 160 µl malachite green reagent, followed by addition of 20 µl 34% sodium citrate, with rapid mixing by vortex after addition of each reagent. The colour develops fully in 1–2 h at room temperature. The concentration of inorganic phosphate was determined from the absorbance at 620 nm according to a standard curve. The actual ATP hydrolysis catalysed by AOX1 was obtained by subtracting ATP self-hydrolysis measured over the same time period.

ATPase assay of crystallized AOX1

Crystals were produced by vapour diffusion in hanging drops containing 1 µl AOX1 (7–10 mg ml^{-1}) and 1 µl crystallization buffer. Sparse matrix screening of crystallization conditions was carried out at 4°C and 16°C using Crystal Screen HR2-110 and Crystal Screen 2 HR2-112 (Hampton Research). In the initial screens, crystals of AOX1 were observed under the following six sets of conditions at 4°C: 0.1 M HEPES buffer, pH 7.5, containing 0.2 M magnesium chloride hexahydrate and 30% v/v 2-propanol; 0.1 M Tris-HCl buffer, pH 8.5, containing 0.2 M ammonium acetate and 30% v/v 2-propanol;

2.0 M sodium chloride and 10% w/v polyethylene glycol 6000; 35% v/v 1,4-dioxane; 25% v/v tert-butanol; and 0.1 M Tris-HCl buffer, pH 8.5, containing 20% v/v ethanol. Crystals appeared within 24 h and remained stable for at least 1 year. The crystallization conditions were further optimized, but the crystals obtained gave poor diffraction, as has been noted previously (Van der Klei *et al*., 1989). AOX1 crystals were recovered from the hanging drop, rinsed in fresh crystallization buffer, and resuspended either in loading buffer for SDS-PAGE analysis, or in the activity assay buffer (50 mM Tris-HCl buffer, pH 7.5 containing 10 mM $MgCl_2$ and 2 mM DTT). The identity of the single band observed by SDS-PAGE was confirmed to be AOX1 by MALDI-TOF MS of the trypsin-digested sample, followed by searching in the NCBInr database. Assay of ATPase activity was performed by addition of 1 mM ATP to the solution of resuspended crystals in assay buffer. After 12 h incubation at 30°C, malachite green reagent was added to detect the production of inorganic phosphate by colour change, in comparison with negative (i.e. buffer only) and positive (i.e. AOX1 prior to crystallization) controls. The amount of protein recovered in crystallized form was too small to be quantified, therefore the assay is qualitative. However, three batches of AOX1 crystals, grown under three different sets of conditions, were tested and all gave positive results for the ATPase assay.

In vitro *amyloid fibril formation*

Amyloid formation of Ure2p in the presence and absence of AOX1 with 1 mM ADP or 1 mM ATP, or without nucleotides, was performed by incubating with shaking at 300 r.p.m. in an Innova 4230 incubator at 30°C (or at 800 r.p.m. on a MS2 Minishaker shaker at 10°C) in Buffer D (25% Buffer B and 75% Buffer C) containing 10 mM $MgCl_2$, 1 mM DTT, 0.02% NaN_3 and a 3 mm-diameter glass bead as described (Zhu *et al*., 2003). The concentration of Ure2p was 30 or 36 μM. If ATP was included, an ATP regenerating system (50 μg ml^{-1} creatine kinase and 8 mM creatine phosphate) was also included in the fibril formation system. The time-course of Ure2p fibril formation was monitored by ThT-binding fluorescence (see below). AOX1 was either present at the start of incubation, or when added later in the time-course of Ure2p fibril formation, the volume change due to addition of AOX1 was less than 4%.

Atomic force microscopy

Atomic force microscopy was used to analyse the change in morphology of Ure2p aggregates over time in the presence or absence of AOX1, and was carried out as described (Jiang *et al*., 2004; Lian *et al*., 2007). Samples were imaged at scan sizes between 1 μm and 10 μm using line scan rates below 2 Hz; 512 × 512 pixels were collected per image. The number of fibrils was counted manually using the software provided with the instrument.

Electron microscopy

A Philips Tecnai 20 electron microscope was used to detect the size and morphology of native AOX1 negatively stained with uranyl acetate (2% w/v).

Intrinsic fluorescence

Intrinsic fluorescence measurements were carried out on a Hitachi F-4500 or a Shimadzu RF-5301PC instrument. Monitoring of ThT-binding fluorescence was performed exactly as described (Zhu *et al*., 2003). The intrinsic florescence spectra of AOX purchased from Sigma and purified AOX1 were compared between 300 and 400 nm, using excitation wavelengths of 280 nm and 295 nm. The proteins were prepared in both Tris buffer (50 mM Tris-HCl, pH 7.5, containing 200 mM KCl and 10 mM $MgCl_2$) and phosphate buffer (50 mM potassium phosphate buffer, pH 7.5). In all cases, the spectra were the same.

Circular dichroism spectroscopy

The far-UV circular dichroism spectra were measured between 190 and 260 nm on a Pistar-180 instrument (Applied Photophysics, UK) at 25°C in a 0.1 mm path-length thermostatted cuvette after pre-incubation for 10 min at 25°C. Spectra of AOX purchased from Sigma and purified AOX1 were compared in Tris buffer (50 mM Tris-HCl, pH 7.5, containing 200 mM KCl and 10 mM $MgCl_2$). The spectra of AOX1 measured in Tris buffer and in phosphate buffer (50 mM potassium phosphate buffer, pH 7.5) were also compared. In all cases, the spectra were identical.

Acknowledgements

We are grateful to Binggen Ru, Peking University, and Gang Liu, Academy of Military Medical Sciences, China, for providing strains. We thank Dr Hui Li for assistance with AFM experiments, Jie Zhuang for assistance with AOX activity assay experiments, Hou-Qing Yu and Dr Xin-Yu Wang for assistance with the Pistar instrument, Peng Xue in the mass spectrometry centre and the staff of the electron microscopy centre for assistance with experiments. This work was supported by the Natural Science Foundation of China (30470363, 30620130109, 30670428), the Chinese Ministry of Science and Technology (2006CB500703, 2006CB910903), and the Chinese Academy of Sciences Knowledge Innovation Project (KSCX2-YW-R-119) (to S.P.). Work performed in the Itzhaki laboratory was supported by the MRC (to L.S.I.), by an EMBO short-term fellowship (to S.P.) and by a Royal Society Joint Project Grant (to L.S.I. and S.P.). Exchange between the Jones and Perrett laboratories was supported by a grant from the China/Ireland Science and Technology Collaboration Research Fund (CI-2004-01). G.W.J. acknowledges the support of the Irish Health Research Board.

References

Bach, S., Talarek, N., Andrieu, T., Vierfond, J.M., Mettey, Y., Galons, H., *et al.* (2003) Isolation of drugs active against mammalian prions using a yeast-based screening assay. *Nat Biotechnol* **21:** 1075–1081.

Bai, M., Zhou, J.M., and Perrett, S. (2004) The yeast prion protein Ure2 shows glutathione peroxidase activity in both native and fibrillar forms. *J Biol Chem* **279:** 50025–50030.

Bodley, A.L., and Jencks, W.P. (1987) Acetyl phosphate as a substrate for the calcium ATPase of sarcoplasmic reticulum. *J Biol Chem* **262:** 13997–14004.

Boero, M., Ikeda, T., Ito, E., and Terakura, K. (2006) Hsc70 ATPase: an insight into water dissociation and joint catalytic role of K+ and Mg2+ metal cations in the hydrolysis reaction. *J Am Chem Soc* **128:** 16798–16807.

Bousset, L., Belrhali, H., Janin, J., Melki, R., and Morera, S. (2001) Structure of the globular region of the prion protein Ure2 from the yeast *Saccharomyces cerevisiae*. *Structure* **9:** 39–46.

Boys, C.W., Hill, D.J., Stockley, P.G., and Woodward, J.R. (1989) Crystallization of alcohol oxidase from *Pichia pastoris*. *J Mol Biol* **208:** 211–212.

Bystrykh, L.V., Dvorakova, J., and Volfova, O. (1989) Alcohol oxidase of methylotrophic thermo- and acido-tolerant yeast *Hansenula sp*. *Folia Microbiol (Praha)* **34:** 233–237.

Chernoff, Y.O., Galkin, A.P., Lewitin, E., Chernova, T.A., Newnam, G.P., and Belenkiy, S.M. (2000) Evolutionary conservation of prion-forming abilities of the yeast Sup35 protein. *Mol Microbiol* **35:** 865–876.

Coffman, J.A., el Berry, H.M., and Cooper, T.G. (1994) The URE2 protein regulates nitrogen catabolic gene expression through the GATAA-containing UASNTR element in *Saccharomyces cerevisiae*. *J Bacteriol* **176:** 7476–7483.

Coschigano, P.W., and Magasanik, B. (1991) The URE2 gene product of *Saccharomyces cerevisiae* plays an important role in the cellular response to the nitrogen source and has homology to glutathione s-transferases. *Mol Cell Biol* **11:** 822–832.

Cregg, J.M., Madden, K.R., Barringer, K.J., Thill, G.P., and Stillman, C.A. (1989) Functional characterization of the two alcohol oxidase genes from the yeast *Pichia pastoris*. *Mol Cell Biol* **9:** 1316–1323.

Danneel, H.J., Reichert, A., and Giffhorn, F. (1994) Production, purification and characterization of an alcohol oxidase of ligninolytic fungus *Peniophora gigantea*. *J Biotechnol* **33:** 33–41.

Douma, A.C., Veenhuis, M., Sulter, G.J., and Harder, W. (1987) A proton-translocating adenosine triphosphatase is associated with the peroxisomal membrane of yeasts. *Arch Microbiol* **147:** 42–47.

Douma, A.C., Veenhuis, M., Waterham, H.R., and Harder, W. (1990) Immunocytochemical demonstration of the peroxisomal ATPase of yeasts. *Yeast* **6:** 45–51.

Dym, O., and Eisenberg, D. (2001) Sequence-structure analysis of FAD-containing proteins. *Protein Sci* **10:** 1712–1728.

Evers, M.E., Harder, W., and Veenhuis, M. (1995) *In vitro* dissociation and re-assembly of peroxisomal alcohol oxidases of *Hansenula polymorpha* and *Pichia pastoris*. *FEBS Lett* **368:** 293–296.

Evers, M.E., Titorenko, V., Harder, W., van der Klei, I.J., and Veenhuis, M. (1996) Flavin adenine dinucleotide binding is the crucial step in alcohol oxidase assembly in the yeast *Hansenula polymorpha*. *Yeast* **12:** 917–923.

Ferard, G., Sall, I., and Metais, P. (1975) Studies on intestinal adenosine triphosphatases. I. Application of a semiautomated method to the rat intestinal brush borders. *Enzyme* **19:** 38–47.

Fernandez-Bellot, E., Guillemet, E., and Cullin, C. (2000) The yeast prion [*URE3*] can be greatly induced by a functional mutated URE2 allele. *EMBO J* **19:** 3215–3222.

Galani, D., Fersht, A.R., and Perrett, S. (2002) Folding of the yeast prion protein Ure2: kinetic evidence for folding and unfolding intermediates. *J Mol Biol* **315:** 213–227.

Gill, S.C., and von Hippel, P.H. (1989) Calculation of protein extinction coefficients from amino acid sequence data. *Anal Biochem* **182:** 319–326.

Goodman, J.M., Scott, C.W., Donahue, P.N., and Atherton, J.P. (1984) Alcohol oxidase assembles post-translationally into the peroxisome of *Candida boidinii*. *J Biol Chem* **259:** 8485–8493.

Gruzman, M.B., Titorenko, V.I., Ashin, V.V., Lusta, K.A., and Trotsenko, Y.A. (1996) Multiple molecular forms of alcohol oxidase from the methylotrophic yeast *Pichia methanolica*. *Biochemistry (Moscow)* **61:** 1537–1544.

Holzmann, K., Schreiner, E., and Schwab, H. (2002) A *Penicillium chrysogenum* gene (*aox*) identified by specific induction upon shifting pH encodes for a protein which shows high homology to fungal alcohol oxidases. *Curr Genet* **40:** 339–344.

Hopkins, T.R., inventor; Phillips Petroleum Corporation, (US) (BR), assignee. (1986) Alcohol oxidase from Pichia-type yeasts. United States Patent 4619898.

Ito, T., Fujimura, S., Uchino, M., Tanaka, N., Matsufuji, Y., Miyaji, T., *et al.* (2007) Distribution, diversity and regulation of alcohol oxidase isozymes, and phylogenetic relationships of methylotrophic yeasts. *Yeast* **24:** 523–532.

Janssen, F.W., Kerwin, R.M., and Ruelius, H.W. (1965) Alcohol oxidase, a novel enzyme from a basidiomycete. *Biochem Biophys Res Commun* **20:** 630–634.

Jiang, Y., Li, H., Zhu, L., Zhou, J.M., and Perrett, S. (2004) Amyloid nucleation and hierarchical assembly of Ure2p fibrils. Role of asparagine/glutamine repeat and nonrepeat regions of the prion domain. *J Biol Chem* **279:** 3361–3369.

Jones, G.W., and Masison, D.C. (2003) *Saccharomyces cerevisiae* Hsp70 mutations affect [*PSI*$^+$] prion propagation and cell growth differently and implicate Hsp40 and tetratricopeptide repeat cochaperones in impairment of [*PSI*$^+$]. *Genetics* **163:** 495–506.

Jones, G.W., and Tuite, M.F. (2005) Chaperoning prions: the cellular machinery for propagating an infectious protein? *Bioessays* **27:** 823–832.

Kato, N., Omori, Y., Tani, Y., and Ogata, K. (1976) Alcohol oxidases of *Kloeckera sp*. and *Hansenula polymorpha*. Catalytic properties and subunit structures. *Eur J Biochem* **64:** 341–350.

Keillor, J.W., and Jencks, W.P. (1996) Phosphorylation of the sodium–potassium adenosinetriphosphatase proceeds through a rate-limiting conformational change followed by rapid phosphoryl transfer. *Biochemistry* **35:** 2750–2753.

Kiess, M., Hecht, H.J., and Kalisz, H.M. (1998) Glucose oxidase from *Penicillium amagasakiense*. Primary structure and comparison with other glucose-methanol-choline (GMC) oxidoreductases. *Eur J Biochem* **252:** 90–99.

Ko, H.S., Fujiwara, H., Yokoyama, Y., Ohno, N., Amachi, S., Shinoyama, H., and Fujii, T. (2005) Inducible production of alcohol oxidase and catalase in a pectin medium by *Thermoascus aurantiacus* IFO 31693. *J Biosci Bioeng* **99:** 290–292.

Kondo, T., Morikawa, Y., and Hayashi, N. (2008) Purification

and characterization of alcohol oxidase from *Paecilomyces variotii* isolated as a formaldehyde-resistant fungus. *Appl Microbiol Biotechnol* **77:** 995–1002.
Kushnirov, V.V., Kochneva-Pervukhova, N.V., Chechenova, M.B., Frolova, N.S., and Ter-Avanesyan, M.D. (2000) Prion properties of the Sup35 protein of yeast *Pichia methanolica*. *EMBO J* **19:** 324–331.
Lee, J.D., and Komagata, K. (1983) Further taxonomic study of methanol-assimilating yeasts with special references to electrophoretic comparison of enzymes. *J Gen Appl Microbiol* **29:** 395–416.
Lian, H.Y., Zhang, H., Zhang, Z.R., Loovers, H.M., Jones, G.W., Rowling, P.J., *et al.* (2007) Hsp40 interacts directly with the native state of the yeast prion protein Ure2 and inhibits formation of amyloid-like fibrils. *J Biol Chem* **282:** 11931–11940.
Loovers, H.M., Guinan, E., and Jones, G.W. (2007) Importance of the Hsp70 ATPase domain in yeast prion propagation. *Genetics* **175:** 621–630.
Lopez-Buesa, P., Pfund, C., and Craig, E.A. (1998) The biochemical properties of the ATPase activity of a 70-kDa heat shock protein (Hsp70) are governed by the C-terminal domains. *Proc Natl Acad Sci USA* **95:** 15253–15258.
Masison, D.C., and Wickner, R.B. (1995) Prion-inducing domain of yeast Ure2p and protease resistance of Ure2p in prion-containing cells. *Science* **270:** 93–95.
Naiki, H., Higuchi, K., Hosokawa, M., and Takeda, T. (1989) Fluorometric determination of amyloid fibrils *in vitro* using the fluorescent dye, thioflavin T1. *Anal Biochem* **177:** 244–249.
Nielsen, L., Khurana, R., Coats, A., Frokjaer, S., Brange, J., Vyas, S., *et al.* (2001) Effect of environmental factors on the kinetics of insulin fibril formation: elucidation of the molecular mechanism. *Biochemistry* **40:** 6036–6046.
Ozimek, P., van Dijk, R., Latchev, K., Gancedo, C., Wang, D.Y., van der Klei, I.J., and Veenhuis, M. (2003) Pyruvate carboxylase is an essential protein in the assembly of yeast peroxisomal oligomeric alcohol oxidase. *Mol Biol Cell* **14:** 786–797.
Ozimek, P., Veenhuis, M., and van der Klei, I.J. (2005) Alcohol oxidase: a complex peroxisomal, oligomeric flavoprotein. *FEMS Yeast Res* **5:** 975–983.
Patel, R.N., Hou, C.T., Laskin, A.I., and Derelanko, P. (1981) Microbial oxidation of methanol: properties of crystallized alcohol oxidase from a yeast, *Pichia sp*. *Arch Biochem Biophy* **210:** 481–488.
Perrett, S., and Jones, G.W. (2008) Insights into the mechanism of prion propagation. *Curr Opin Struct Biol* **18:** 52–59.
Perrett, S., Freeman, S.J., Butler, P.J., and Fersht, A.R. (1999) Equilibrium folding properties of the yeast prion protein determinant Ure2. *J Mol Biol* **290:** 331–345.
Rai, R., Tate, J.J., and Cooper, T.G. (2003) Ure2, a prion precursor with homology to glutathione S-transferase, protects *Saccharomyces cerevisiae* cells from heavy metal ion and oxidant toxicity. *J Biol Chem* **278:** 12826–12833.
Roa, M., and Blobel, G. (1983) Biosynthesis of peroxisomal enzymes in the methylotrophic yeast *Hansenula polymorpha*. *Proc Natl Acad Sci USA* **80:** 6872–6876.
Roberts, B.T., Moriyama, H., and Wickner, R.B. (2004) [*URE3*] prion propagation is abolished by a mutation of the primary cytosolic Hsp70 of budding yeast. *Yeast* **21:** 107–117.
Roggenkamp, R., Janowicz, Z., Stanikowski, B., and Hollenberg, C.P. (1984) Biosynthesis and regulation of the peroxisomal methanol oxidase from the methylotrophic yeast *Hansenula polymorpha*. *Mol Gen Genet* **194:** 489–493.
Rowlands, M.G., Newbatt, Y.M., Prodromou, C., Pearl, L.H., Workman, P., and Aherne, W. (2004) High-throughput screening assay for inhibitors of heat-shock protein 90 ATPase activity. *Anal Biochem* **327:** 176–183.
Sadis, S., and Hightower, L.E. (1992) Unfolded proteins stimulate molecular chaperone Hsc70 ATPase by accelerating ADP/ATP exchange. *Biochemistry* **31:** 9406–9412.
Sambrook, J., Fritsch, E.F., and Maniatis, T. (1989) *Molecular Cloning: A Laboratory Manual*, 2nd edn. Cold Spring Harbor, NY: Cold Spring Harbor Laboratory Press.
Schwimmer, C., and Masison, D.C. (2002) Antagonistic interactions between yeast [*PSI*$^+$] and [*URE3*] prions and curing of [*URE3*] by Hsp70 protein chaperone Ssa1p but not by Ssa2p. *Mol Cell Biol* **22:** 3590–3598.
Shorter, J., and Lindquist, S. (2005) Prions as adaptive conduits of memory and inheritance. *Nat Rev Genet* **6:** 435–450.
Sibirny, A.A., Titorenko, V., Efremov, B.D., and Tolstorukov, I.I. (1987) Multiplicity of mechanisms of carbon catabolite repression involved in the synthesis of alcohol oxidase in the methylotrophic yeast *Pichia pinus*. *Yeast* **3:** 233–241.
Silver, J.M., and Eaton, N.R. (1969) Functional blocks of the ad-1 and ad-2 mutants of *Saccharomyces cerevisiae*. *Biochem Biophys Res Commun* **34:** 301–305.
Taylor, K.L., Cheng, N., Williams, R.W., Steven, A.C., and Wickner, R.B. (1999) Prion domain initiation of amyloid formation *in vitro* from native Ure2p. *Science* **283:** 1339–1343.
Thual, C., Komar, A.A., Bousset, L., Fernandez-Bellot, E., Cullin, C., and Melki, R. (1999) Structural characterization of *Saccharomyces cerevisiae* prion-like protein Ure2. *J Biol Chem* **274:** 13666–13674.
Thual, C., Bousset, L., Komar, A.A., Walter, S., Buchner, J., Cullin, C., and Melki, R. (2001) Stability, folding, dimerization, and assembly properties of the yeast prion Ure2p. *Biochemistry* **40:** 1764–1773.
Titorenko, V.I., and Rachubinski, R.A. (2000) Peroxisomal membrane fusion requires two AAA family ATPases, Pex1p and Pex6p. *J Cell Biol* **150:** 881–886.
Tribouillard-Tanvier, D., Béringue, V., Desban, N., Gug, F., Bach, S., Voisset, C., *et al.* (2008) Antihypertensive drug guanabenz is active in vivo against both yeast and mammalian prions. *PLoS ONE* **3:** e1981.
Umland, T.C., Taylor, K.L., Rhee, S., Wickner, R.B., and Davies, D.R. (2001) The crystal structure of the nitrogen regulation fragment of the yeast prion protein Ure2p. *Proc Natl Acad Sci USA* **98:** 1459–1464.
Van der Klei, I.J., Lawson, C.L., Rozeboom, H., Dijkstra, B.W., Veenhuis, M., Harder, W., and Hol, W.G. (1989) Use of electron microscopy in the examination of lattice defects in crystals of alcohol oxidase. *FEBS Lett* **244:** 213–216.
Veenhuis, M., Harder, W., van Dijken, J.P., and Mayer, F. (1981) Substructure of crystalline peroxisomes in methanol-grown *Hansenula polymorpha*: evidence for an *in vivo* crystal of alcohol oxidase. *Mol Cell Biol* **1:** 949–957.

Veenhuis, M., Van Dijken, J.P., and Harder, W. (1983) The significance of peroxisomes in the metabolism of one-carbon compounds in yeasts. *Adv Microb Physiol* **24:** 1–82.

Wickner, R.B. (1994) [*URE3*] as an altered URE2 protein: evidence for a prion analog in *Saccharomyces cerevisiae*. *Science* **264:** 566–569.

Wickner, R.B., Masison, D.C., and Edskes, H.K. (1995) [*PSI*$^{+}$] and [*URE3*] as yeast prions. *Yeast* **11:** 1671–1685.

Wickner, R.B., Edskes, H.K., Shewmaker, F., and Nakayashiki, T. (2007) Prions of fungi: inherited structures and biological roles. *Nat Rev Microbiol* **5:** 611–618.

Zadorskii, S.P., Sopova, IuV., and Inge-Vechtomov, S.G. (2000) Prionization of the *Pichia methanolica* SUP35 gene product in the yeast *Saccharomyces cerevisiae*. *Genetika* **36:** 1322–1329.

Zhang, Z.R., Bai, M., Wang, X.Y., Zhou, J.M., and Perrett, S. (2008) 'Restoration' of glutathione transferase activity by single-site mutation of the yeast prion protein Ure2. *J Mol Biol* **384:** 641–651.

Zhu, L., Zhang, X.J., Wang, L.Y., Zhou, J.M., and Perrett, S. (2003) Relationship between stability of folding intermediates and amyloid formation for the yeast prion Ure2p: a quantitative analysis of the effects of pH and buffer system. *J Mol Biol* **328:** 235–254.

